Undesirable contaminants possibly introduced in LiNbO$_3$ electro-optic devices

Hirotoshi Nagata,[a)] Naoki Mitsugi, and Toshihiro Sakamoto

Optoelectronics Research Division, New Techaology Research Laboratories.
Sumitomo Osaha Cement Company, Ltd.. 585 Toyotomi-cho. Fuaabashi-shi, Chiba 274-8601, Japan

Kaori Shima, Masumi Tamai, and Eungi Min Haga

Advanced Materials Research Division, New Technology Research Laboratories, Sumitomo Osaka Cement Company, Ltd.. 585 Toyotomi-cho, Fanabashi-shi. Chiba 274-8601. Japan

Inorganic contaminants in the fabrication of LiNbO$_3$ optical waveguide devices are examined with regard to their effect on the ultimate device performance and quality. We find a possibility that some chemicals such as a photoresist developer, etc., Ieave contaminants including silicon and alkalis on the LiNbO$_3$ wafer, and result in an increase of light propagation loss, a pealing of the SiO$_2$ layer from the wafer, and a large dc drift. © *1999 American Institute of Physics.*
[SOO21-8979(99)08023-8]

. INTRODUCTION

Since LiNbO$_3$-based optical waveguide modulators are widely used in global fiber communication systems, their long-term reliability has been carefully investigated from the viewpoint of the stability of the device performance, such as dc drift phenomena. For instance, the latest Bellcore GR-468-CORE standard comments on the reliability and quality requirements for LiNbO$_3$ modulators in addition to conventional laser devices.[1] However, reports on problems in device quahty due to the LiNbO$_3$ modulator fabrication processes are limited, although a demand for LiNbO$_3$ modulators is rapidly increasing. The purpose of this article is to reveal such problems and provide experimental information to investigate the LiNbO$_3$ device quality; especially, the effect of process-induced contaminants to device performance. Some of the data have been obtained by root-cause analyses of actually failed devices. Our examination is mainly focused on silicon and alkali contaminants due to chemical treatments of LiNbO$_3$ wafers because they are found to cause catastrophic failures such as dc drift of the optical output signal, break of rf electrodes on the suface, etc.

. STRUCTURE OF TYPICAL LiNbO$_3$ MODULATOR

Figure 1 shows a schematic cross section of the LiNbO$_3$ waveguide modulators, mainly consisting of a LiNbO$_3$ substrate with buried optical waveguides, a SiO$_2$ buffer layer covering the LiNbO$_3$ surface, and gold electrodes with more than 20 μm thickness. The optical waveguides were formed by thennal diffusion of metallic Ti lines at approximately 1000°C in a wet oxidizing atmosphere. The patterning of Ti lines was performed using conventional photolithography and a film deposition technique; e.g., Iift-off of the Ti film. After the waveguide formation, the SiO$_2$ Iayer was deposited by a vacuum evaporation method and annealed at 600°C in

oxygen atmosphere. This oxygen annealing is an essential process to fully oxidize the deposited layer and decrease dc drift phenomena in the device. On the SiO$_2$ surface, a Au/Ti binary film was deposited by sequential vacuum evaporation of Ti and Au, as a glue layer for the thick Au electrodes prepared by an electroplating method. The role of the Ti layer is to increase the bonding strength of the Au layer to the SiO$_2$: a Cr layer is applied similarly instead of the Ti. The Au electrodes were grown between the photoresist walls which had been patterned on the Au/Ti binary layer, and these photeresists were chemically removed. At the last process, the Au/Ti binary layer left between the Au electrodes was chemically etched to expose the SiO$_2$ surface as shown in Fig. 1.

In the above-mentioned fabrication process of LiNbO$_3$ devices, some chemicals for wet processes may contaminate the device constituent materials, especially the LiNbO$_3$ wafer surface and SiO$_2$ buffer layer. For instance, there is a possibility that an inorganic-based photoresist developer, including sodium silicates, Ieaves Si-based contaminants on the LiNbO$_3$ wafers before the waveguide diffusion process at high temperatures. As described in Sec. III, the Si contaminants were found to cause an anomaly in the waveguide morphology, Ieading to an increase of optical propagation losses. Alkali contaminants, such as Na and K, are supplied to the SiO$_2$ buffer layer from photoresist developers, detergent for wafer cleaning, etc., and deteriorate not only the bonding strength of the SiO$_2$ film to LiNbO$_3$ but also the dc stability of the device (Sec.IV). The dc stability (dc drift) is effected also by contaminants left on the SiO$_2$ surface between the pair of electrodes. If the process consists of the deposition of metallic Ti (or Cr) film on the SiO$_2$, there is the possibility that a partially oxidized Ti (or Cr) thin layer is left on the SiO$_2$ even after etching the metal layer (Sec. V). The following sections show examples of the process-induced contamination, based on failure-cause analyses of actual LiNbO$_3$ modulators.

[a)]Electronic mail: hinagata@sits.soc.co.jp
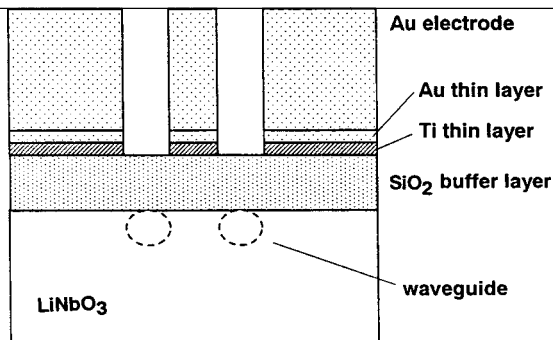
FIG. 1 . Schematic illustration of the cross section of LINbO₃ electro-optic devices.

. WAVEGUIDE ROUGHENING DUE TO Si CONTAMINANTS

A. Si-based contaminants on LiNbO₃ Waveguides

Silicon-based compounds are contained in an abradant (e.g., colloidal silica) for polishing LiNbO₃ wafers and in some inorganic-based chemicals (e.g., sodium silicates) for developing photoresist on the wafer. Generally, these materials can be removed completely from the wafer surface by common cleaning processes, and Si contaminants rarely cause device failure. Figure 2(a) shows an example of such an uncommon fajilure; a scanning electron microscopic (SEM) image of the failed waveguide surface. The waveguides were prepared on z-cut LiNbO₃ wafers by a Ti-indiffusion technique. Normal LiNbO₃ waveguides have a surface as shown in Fig. 2(b), which consist of a waveguide almost corresponding to a trace of the deposited Ti line and a pair of bands formed on both sides of the waveguide. Nozawa and Miyazawa reported that generation of a dislocation in LiNbO₃ crystal due to the Ti-indiffusion caused such bands along the waveguide.[2] However, as shown in Fig. 2(a), the failed waveguide did not accompany the dislocation bands and had many precipitates in it. On the other hand, the
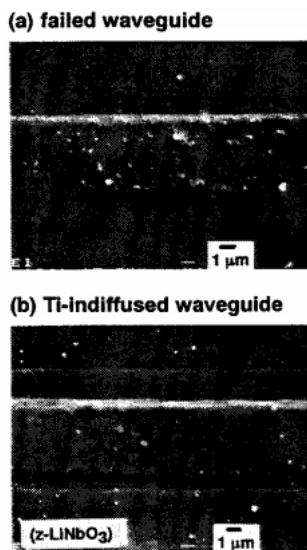
FIG. 2. SEM images of failed optical waveguide (a) and ordinary waveguide (b) formed on z-cut LiNbO₃ by the Ti-indiffusion process.
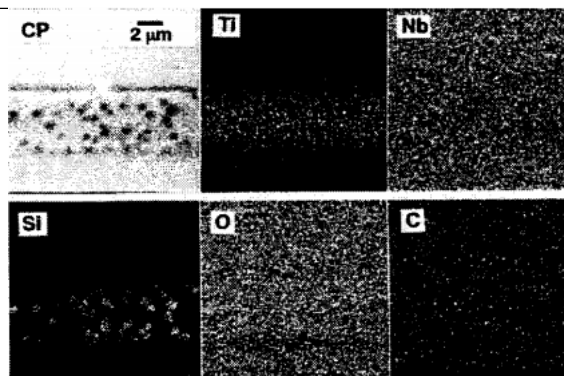
FIG. 3. Planar distribution images Ti, Nb, Si, O, and C of the failed waveguide of Fig. 2 observed by analyiic SEM. The image marked by "CP" reveals a chemical compositional image.

failed waveguides exhibited much larger optical propagation loss than normal waveguides; excess losses in the order of several dB.

Figure 3 shows analytical SEM images of the failed waveguide, in which planar distributions of Ti, Nb, Si, O, and C are exhibited. The image denoted by "CP" exhibits the chemical composition of the surface; brighter contrast for the region consisting of heavier elements. The region with many Ti signals detected corresponds to the Ti-indiffused waveguide. From Figs. 2 and 3, the precipitates on the fajiled waveguide are expected at least to be composed of silicon oxides.

B. Structural analysis of precipitates

In order to identify the precipitate material, we carried out differential thermal analysis (DTA) and x-ray diffractometry (XRD) analysis on a LiNbO₃ /SiO₂ powder mixture because the actual precipitates in the faiiled waveguides were too small for analyses. From the analysis results, we considered that the precipitates were mainly SiO₂ rather than a compound of LiNbO₃ and SiO₂.

Figure 4 shows DTA profiles for powder samples of SiO₂ , LiNbO₃ , and the LiNbO₃ /SiO₂ mixture (1 : 1 in weight ratio). The powders were prepared by grinding the LiNbO₃ wafer and SiO₂–glass granules (a vacuum evaporation
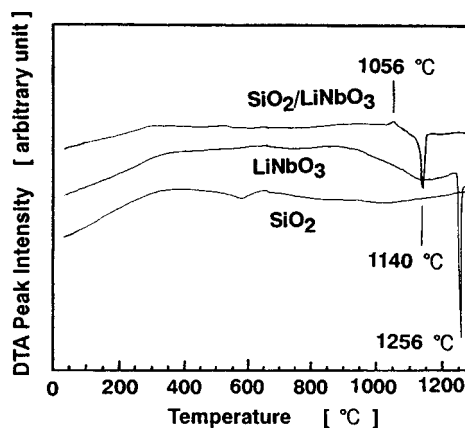
FIG. 4. DTA profiles on a SiO₂ /LiNbO₃ powder mixture, a LiNbO₃ powder, and a SiO₂ powder.

(a) SiO$_2$/LiNbO$_3$ after heat treatment up to 1300 °C

● tridymite

(b) LiNbO$_3$ after heat treatment up to 1300 °C

2 θ   [degree]
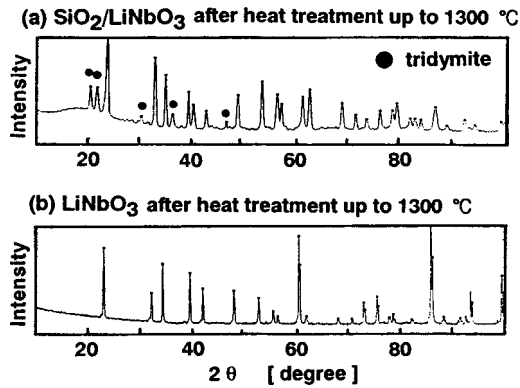
FIG. 5. XRD peak profiles on a SiO$_2$/LiNbO$_3$ powder mixture (a) and a LiNbO$_3$ powder (b) measured after their DTA of Fig. 4.

source). DTA measurements were performed using the 10 mg sample in flowing air (200 cm^3/min) from 30 to 1 300°C at a heating rate of 10 K/min. The large endothennic peak at 1256°C of the LiNbO$_3$ sample denotes the congruent melting temperature of LiNbO$_3$, which was reported to be 1253°C.[3] A specific feature in the DTA profile of the LiNbO$_3$/SiO$_2$ nnxture was the decrease of the melting temperature from 1256 to 1146 °C and the appearance of a broad
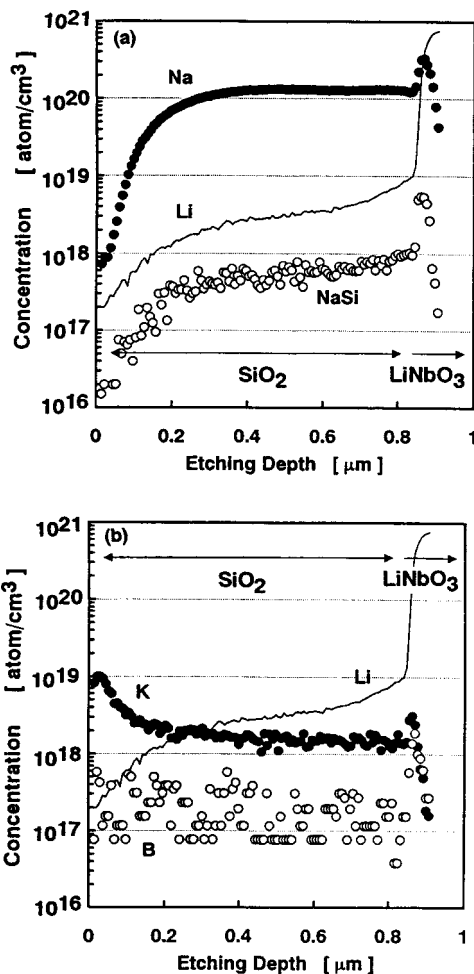
TABLE I. Chemical composition at the boundary between the SiO$_2$ film and z-cut LiNbO$_3$ substrate measured by SIMS (in at. %).

	Li	Nb	Si	O	C	Na
SiO$_2$ bottom	3.1	3.8	21.2	52.1	17.4	2.4
LiNbO$_3$ surface	10.0	17.7	0.6	50.5	19.9	1.3

exothermic peak at 1056°C. The cause of what was seen in the former observation may be a change of the Li/Nb ratio in LiNbO$_3$, judging from the equilibrium diagram of the LiNbO$_3$ system: melting points at 35 and 60 mol % Li$_2$O contents are 1190 and 1160°C, respectively.[3] There is the possibility that some amount of Li and/or Nb diffased into SiO$_2$ from LiNbO$_3$ during heating. The origin of the peak at l056°C is not known.

After DTA measurements, the powder samples were analyzed by XRD to check their crystal structures. Figures 5(a) and 5(b) show XRD results of the LiNbO$_3$/SiO$_2$ mixture and LlNbO$_3$, respectively. As is seen in Fig. 5(a), the diffraction peaks of LiNbO$_3$ broadened due to the heat treatment with SiO$_2$ at over 1000°C and additional peaks of tridymite-type SiO$_2$ appeared (black circles). We consider that LiNbO$_3$ crystallites were partially decomposed by a chemical reaction with SiO$_2$ at high temperatures, as revealed by the DTA measurements, and caused the broadening of the XRD peaks.

The above results suggest that Si-based contaminants on the LiNbO$_3$ wafer caused the growth of tridymite-type SiO$_2$ and partial decomposition of LiNbO$_3$ during the heat treatment for waveguide formation. Thus, the precipitates that appeared on the failed waveguide [Fig. 2(a)] are thought to be tridymite particles. Further, the decomposition of LiNbO$_3$ crystallites is considered to relax the surface strain (i.e., dislocation) caused by Ti diffusion and suppress the generation of dislocation-induced bands along both sides of the waveguide, as shown in Fig. 2(a).

FIG. 6. SIMS measurement results on the SiO$_2$ buffer layer of the failed device. In this device, a bonding strength of the SiO$_2$ layer to LiNbO$_3$ was extraordinarily weak and a large dc drift was observed.
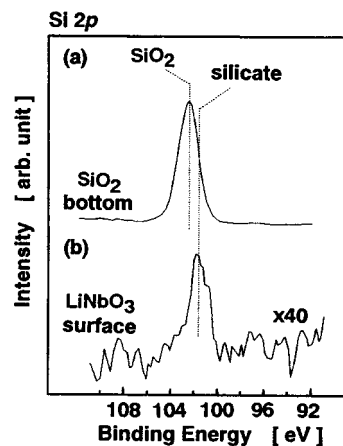
FIG. 7. Comparison of Si 2p XPS peaks from the exposed SiO$_2$ film bottom (a) and the exposed LiNbO$_3$ substrate surface (b).
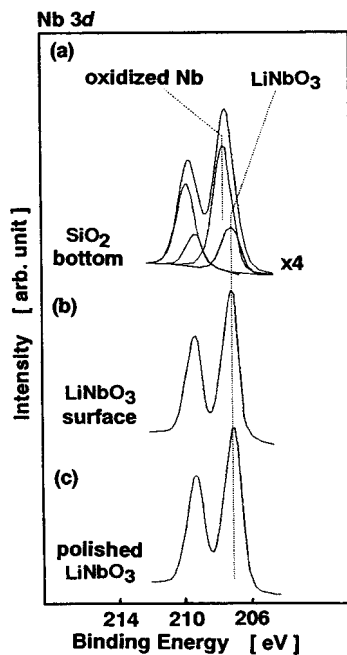
FIG. 8. Comparison of Nb $3d$ XPS peaks from the exposed SiO_2 film bottom (a), the exposed $LiNbO_3$ substrate surface (b), and the polished $LiNbO_3$ surface (c).

FIG. 9. Comparison of Li $1s$ XPS peaks from the exposed SiO_2 film bottom (a), the exposed $LiNbO_3$ substrate surface (b), and the polished $LiNbO_3$ surface (c).

. BUFFER LAYER PEELING DUE TO ALKALI CONTAMINANTS

A. Alkali contaminants in SiO_2/$LiNbO_3$ interface

Considering the chemistry of the film interfaces is essential to investigating device fajilures. In $LiNbO_3$ devices, the peeling of the SiO_2 Iayer from the $LiNbO_3$ substrate occurs sometimes during the machining or assembly processes of the device chip. As the main cause of such failures, alkali contaminants (Na and K) were found to exist at the SiO_2 /$LiNbO_3$ mterface as shown in Figs. 6(a) and 6(b); secondary ion mass spectrometry (SIMS) results on a defective SiO_2 buffer layer. Both Na and K ions were found to be contained in photoresist developers as a sodium silicate and a potassium borate, which were used in the device fabrication process. One of the developers including Na was used on the LiNb03 wafer surface before the SiO_2 film deposition, and another developer including K was used on the SiO_2 surface after the film annealing at 600℃ in flowing O_2 atmosphere. There is the possibility that both photoresist developers were incompletely removed and diffused throughout the SiO_2 layer due to the heat process. Because LiNb03 has an affinity for alkalis, contaminants might concentrate at the SiO_2 /$LiNbO_3$ mterface. With respect to this failed sample, the amount of Na contaminant ions was much higher than the Li ions diffusing from $LiNbO_3$ mto the SiO_2 layer.

We also examined the same interface with an x-ray photoelectron spectrometer (XPS). After peeling the defected SiO_2 Iayer from $LiNbO_3$, the samples were immediately placed in the XPS analyzer for examination of the exposed interface. Table I shows a list of elements detected from the interfaces: the SiO_2 film side and $LiNbO_3$ substrate side. The XPS result revealed the existence of Na at the interface. Considering the molar volume of LiNb03 the amount of Na de-

tected by XPS (2 at. %) was estimated to be 1×10^{21} atoms/cm^3 and consistent with the SIMS result.
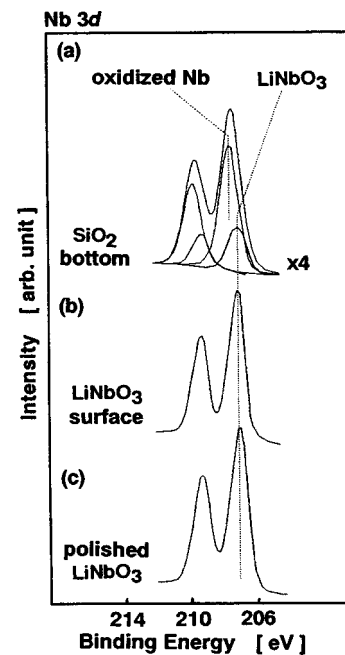
B. Chemical and structural analyses of SiO_2/$LiNbO_3$ interface

Figure 7 shows a comparison of Si $2p$ XPS peaks from (a) the exposed SiO_2 film bottom and (b) the exposed $LiNbO_3$ substrate surface. The binding energy in the horizontal axes was calibrated using a particular C peak energy which was detected from the same samples. Although the Si $2p$ peak obtained from the film bottom was dominantly assigned to SiO_2 , the peak from the substrate surface showed l eV Iower binding energy, which is possibly due to a presence of silicate compounds. A similar comparison to Nb $3d$ and Li $1s$ peaks is shown in Figs. 8 and 9, respectively. Data measured from the polished $LiNbO_3$ surface (c) is also shown in Figs. 8 and 9. The Nb $3d$ peaks from the SiO_2 film bottom [Fig. 8(a)] consisted of two different peaks and were decomposed into the pair of Nb peaks due to $LiNbO_3$, while the other pair had a binding energy of 0.5 eV higher. The additional pair is estimated to be caused by oxidized Nb, such as Nb_2O_5 , because the Nb $3d_{5/2}$ Peak from N_2O_5 is known to appear from 206 to 208 eV, while the peak from $LiNbO_3$ appears at 207 eV.[4] We consider that the above XPS results demonstrate the possibility of the formation of Nb-based silicates at the boundary.

Then, in order to examine the physical structure of the defected interface, a transmission electron microscopic (TEM) observation was carried out on a cross section of the sample. Figure 10 shows the cross-sectional TEM image of the SiO_2 /$LiNbO_3$ mterface observed at an electron-beam acceleration energy of 300 kV. The boundary was found to extend parallel to the [110] direction and normal to the [001] direction (z axis) of $LiNbO_3$. The gap between each of the
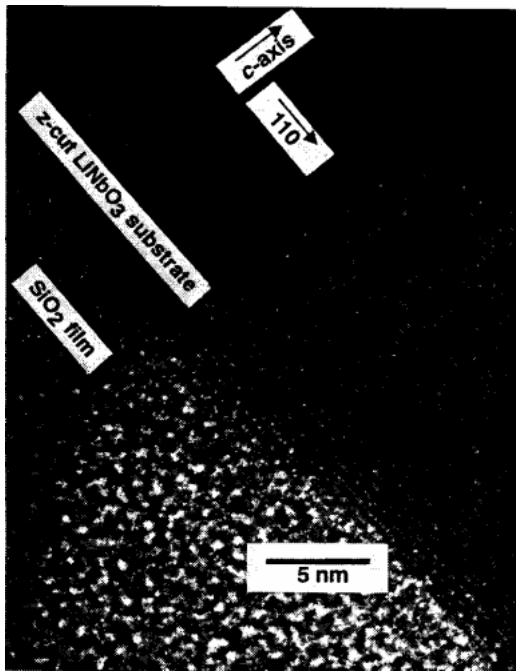
FIG. 10. Cross-sectional TEM image of the SiO$_2$/LiNbO$_3$ boundary.

FIG. 11 . SIMS results with respect to Ti and Cr elements measured on the sample of Fig. 6.

bright lines appearing in the lattice image of the substrate was measured to be 0.466 nm, corresponding to 0.462 nm for the distance between the (OO3) planes of LiNbO$_3$. As exhibited, LiNbO$_3$ appears to maintain its crystal structure at the boundary to the SiO$_2$ film without any distortion of the lattice or growth of other crystalline materials. The state of the SiO$_2$ film was shown to be amorphous, and no additional stucture was found at the interface.

C. Effect of alkali to Si02 film bonding strength

As shown in Fig. 6, Li ions diffused throughout the SiO$_2$ film from the LiNbO$_3$ substrate with a concentration of 1 × 10^{18}–1 × 10^{19} atom/cm^3. Considering the SiO$_2$ film thickness, the amount of Li ions supplied from LlNbO$_3$ to the SiO$_2$ film were roughly estimated to be in the order of 1 × 10^{14} atom/cm^2, corresponding to one third or less of the ions in the LiNbO$_3$ unit cell. In other words, because the LiNbO$_3$ crystal consists of six layers of anions and vacancy divided by O-O planes along its z axis (1.3 nm length), there is the possibility that the top-surface layer of the z-cut LiNbO$_3$ substrate, corresponding to the gap distance of the (003) planes, decomposed during the SiO$_2$ film deposition and its annealing. This estimation is supported by the TEM observation results in Fig. 10. The Na ions were additionally introduced into the SiO$_2$ Iayer in the failed sample.

Judging from the above SIMS, XPS, and TEM analysis results, the bonding force of the SiO$_2$ film to LiNbO$_3$ is considered to be the formation of the Nb silicates; a partial substitution of Si by Nb of the Si-O-Si network. On the other hand, the alkalis seemed not to generate structural anomalies such as extra fine crystallites at the interface, and to diffbse into the Si-O-Si network. Because alkali ions tend to be interstitially trapped in the Si-O-Si network, if the alkali concentration is increased, a number of Si-O-Nb
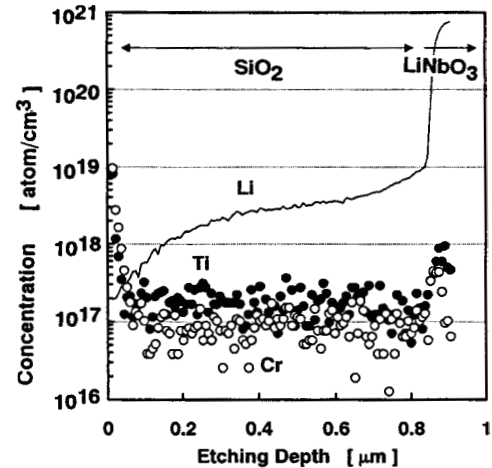
bonds at the interface might be reduced in order to maintain a neutral electrical charge. As a result, the bonding strength of SiO$_2$ /LiNbO$_3$ rs thought to be largely weakened by external alkali contaminants such as Na$^+$ and K$^+$ in addition to the intrinsic Li$^+$ contaminant.
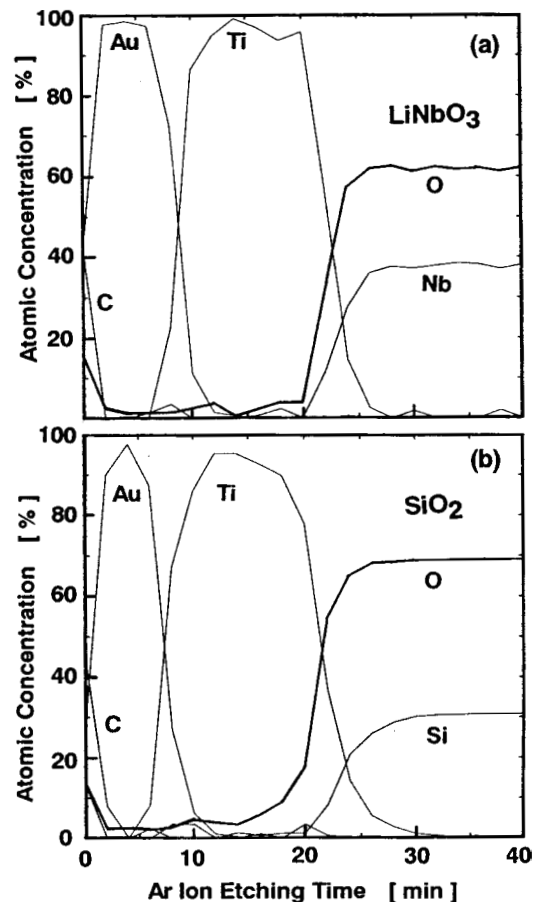
FIG. 12. XPS depth profiles measured on the Au/Ti binary films deposited on the LiNbO$_3$ single-crystal substrate (a) and on the SiO$_2$ layer covering LiNbO$_3$ (b). C is, O 1s, Au 4f, Ti 2p, Nb 3d, and Si 2p XPS peaks were used for the measurements.
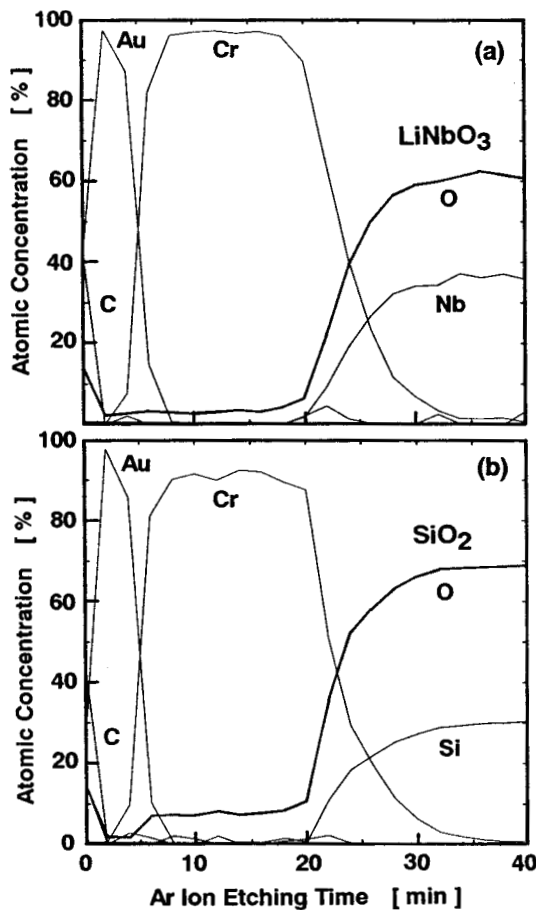
FIG. 13. XPS depth profiles measured on the Au/Cr binary films deposited on the $LiNbO_3$ single-crystal substrate (a) and on the SiO_2 Iayer covering $LiNbO_3$ (b). C is. O Is, Au 4*f*. Cr 2*p*, Nb 3*d*, and Si 2*p* XPS poaks were used for the measurements.

. ELECTRICAL ANOMALY OF SiO_2 DUE TO METALLIC CONTAMINANTS

A. Ti and Cr residue on SiO_2 buffer layer surface

As described in Sec. II, a thin metal film such as Ti, Cr is inserted between the SiO_2 buffer layer and Au electrodes to increase their adhesive strength. Further, the Cr film is sometimes used as an etching mask for the reactive plasma etching of SiO_2 and/or $LiNbO_3$ because of its slower etching rate against the etchant (such as fluorocarbon plasma). For instance, a 200-nm-thick Cr film was enough as the etching mask for about a 1-/1;m-deep etching of SiO_2 by electron cyclotron resonance (ECR) plasma etching with CF_4. After the processes, if it is also prepared on the surface between the electrodes, the metal film is chemically removed (wet etching).

In order to keep the device performance stable, such a metallic layer must be completely removed from the oxide surface. However, sometimes small amounts of metal elements are left on the surface as shown in Fig. 11. Figure 11 shows SIMS analysis results of the faiiled device (the same device as in Fig. 6), in which the Ti and Cr residue on the SiO_2 surface is revealed. This failed device performed a large dc drift phenomenon even at room temperature. We thought that the Ti and Cr residue was also the cause of the

dnft in addition to the alkali contaminants in SiO_2. In this device, Cr was deposited on SiO_2 as the etching mask for the plasma etching process, and Ti was used as the glue layer for Au electrode fonnation. The examined position was the surface exposed between the pair of electrodes, which had been treated by chemicals to remove the metals.

As the cause of the condensation of metallic elements at the suface, we considered two possibilities; one due to the process and another due to the materials' nature. There is the possibility that the chemical which solves metallic elements soaked into the SiO_2 film and dried. Another possibility is, for instance, that the Ti and Cr films decreased their solubility at the interface with SiO_2 due to oxidization. Optimization of the chemical treatment conditions, such as the rinse procedure, is effective in reducing defective devices and must be investigated. Here, the possible chemical reaction at the interface was examined to provide information for process optimization.

B. Chemical reactions of Ti and Cr films with $LiNbO_3$ and SiO_2 substrates

We examined the chemical reaction at the interfaces of $Ti/LiNbO_3$, $Cr/LiNbO_3$, Ti/SiO_2, and Cr/SiO_2 using XPS. Because in x-cut $LiNbO_3$ devices the metal film is directly deposited on the $LiNbO_3$ crystal, the interface with $LiNbO_3$ was also examined in addition to the interface with the SiO_2 film. Conceming the chemical reactions at the interface, the chemical equilibrium diagram on the oxidization of metals suggests that metallic Ti has the strongest oxygen affinity and combined into TiO, and a reaction from TiO into Ti_2O_3, competes with the oxidation of Si into SiO_2.[5] The oxygen affinity of metallic Cr is the weakest, and the reaction from Cr into Cr_2O_3 competes with the oxidation of Ti_2O_3 into Ti_3O_5, and from NbO_2 mto NbO. From this information, the Ti film is expected to more strongly combine with the $LiNbO_3$ and SiO_2 substrates via oxygen, than the Cr film.

In order to evaluate the chemical reaction at the TVLiNbO_3, Ti/SiO_2, $Cr/LiNbO_3$, and Cr/SiO_2 interfaces, Au/Ti and Au/Cr binary films were prepared on a $LiNbO_3$ single crystal and on the SiO_2 Iayer covering the $LiNbO_3$ by conventional vacuum evaporation deposition at about 200°C. For preparation of the latter samples, the 1-μm-thick SiO_2 Iayer on $LiNbO_3$ had been deposited by vacuum evaporation deposition and annealed at 600°C under O_2 atnosphere. The depositions of Ti (Cr) and Au layers were performed sequentially without breaking the vacuum. The film thickness was designed to be approximately 50 nm for Ti and Cr, and approximately 35 nm for Au. The Au film was deposited to eliminate the oxidization of the thin Ti and Cr films from their surface after the deposition. The interfaces were examined by XPS using monochromatic Al *K* radiation and an Ar-ion etching technique for the depth profile.

Figures 12 and 13 show XPS depth profiles measured on Au/Ti and Au/Cr binary films, respectively, in which (a) denotes the films on $LiNbO_3$ and (b) the films on the SiO_2 layer covering the $LiNbO_3$. The vertical axis is plotted by the atomic concentration in percent. The horizontal axis is plotted by the Ar-ion etching times. As is seen, both Ti and Cr
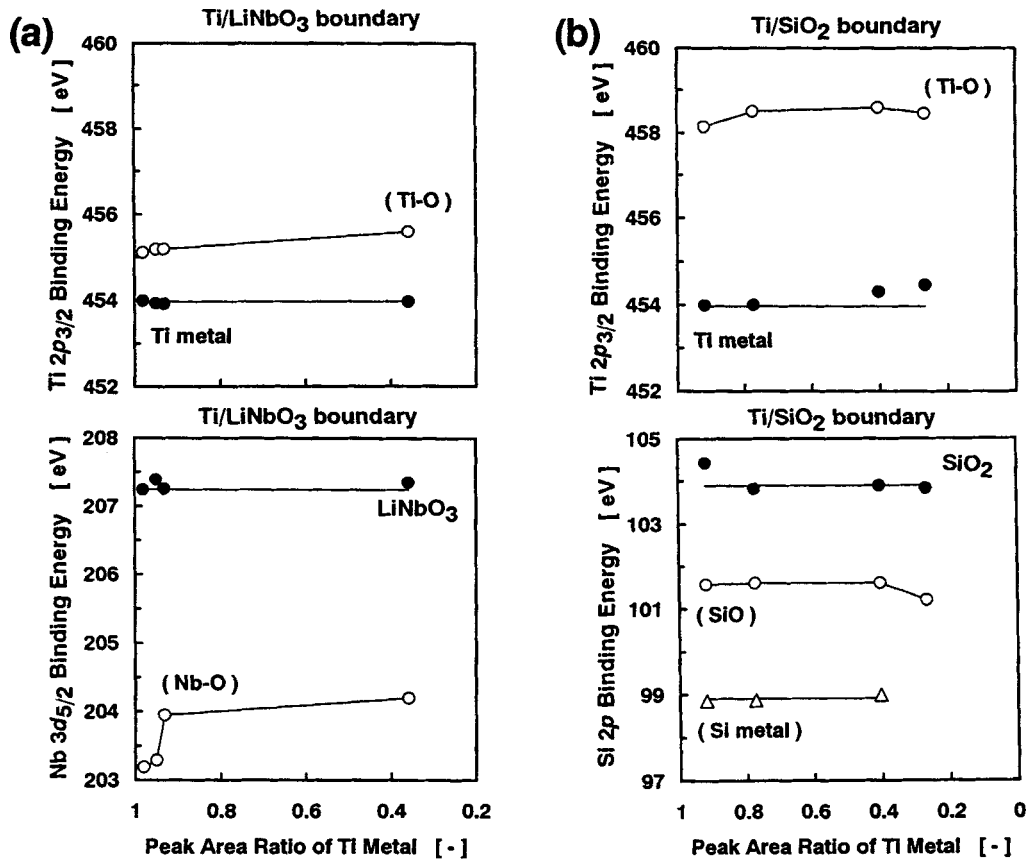
FIG. 14. XPS chemical shift measured on Ti $2p_{3/2}$ and Nb $3d_{5/2}$ peaks of the Ti/LiNbO$_3$ sample (a) and on Ti $22p_{3/2}$ and Si $2p$ of the Ti/SiO$_2$/LiNbO$_3$ sample (b). The data were obtained at the points after 20, 22. 24, and 26 min of Ar-ion etching of Figs. 1 (a) and 1 (b) for the concsponding sample. The horizontal axes are plotted by an XPS peak area ratio of the metallic component not by the sputtering time calculated by (Ti $2p$)$_{metal}$/[(Ti $2p$)$_{metal}$ +(Ti $2p$)$_{oxides}$].

films were partially oxidized possibly due to the transportation of oxygen from the substrates. The average contents of oxygen through the film were larger in the films on the SiO$_2$ layer (5-10 at. %) than the films on the LiNbO$_3$ crystal (<5 at. %). Because the SiO$_2$ Iayer prepared by vacuum evaporation deposition was less in density and adsorbed a lot of H$_2$O (-OH), the penetration of oxygen into the film might have been intensified.

On the same samples, the chemical shift of the XPS peaks was examined and is shown in Figs. 14 and 15, respectively; (a) for the LiNbO$_3$ substrate and (b) for the SiO$_2$ layer. The upper graphs show the chemical state of Ti (Fig. 14) and Cr (Fig. 15), and the lower graphs show the state of Nb (a) and Si (b). The data were obtained at the points after 20, 22, 24, and 26 min of Ar-ion etching (see Figs. 12 and 13). However, because the etching rate depends on the material, the horizontal axes of Figs. 14 and 15 were plotted by the XPS peak area ratio of the metallic component, not by the sputtering time; e.g., (Ti $2p$)$_{metal}$/ [(Ti $2p$)$_{metal}$+(Ti $2p$)$_{oxides}$]. The left side of the axis corresponds to the metal layer, while the right side to the substrate. Judging from the point of the general tendency of the binding energy of the XPS peak from the metals shifts to be higher after their oxidization, a degree of oxidization at the boundary was higher in the films on the SiO$_2$ layer than those on LiNbO$_3$, as expected from the oxygen contents in the films. From the viewpoint of the oxygen affinity of met-

als, the data revealed that the Ti took greater amounts of oxygen from the substrate and is consistent with the thermal equilibrium diagram.[5] Note that the SiO$_2$ film surface was reduced into metallic Si due to the Ti deposition. Further, at the Ti/SiO$_2$ mterface, the oxidized state of Ti was found to change sharply while the Cr was gradually oxidized.

The above results are summarized in Table ll, in which the oxygen contents in the films were evaluated again by Auger electron spectrometry (AES) and are similar to the XPS results. Table II also shows data on the surface morphology of the Au film covering the Ti and Cr films obtained by atomic force microscopy (AFM). Only the Au/Ti/LiNbO$_3$ sample exhibited a specific surface texture, with a smoother surface consisting of large Au grains. These results suggest that the oxidization of the Ti and Cr films occurred during their growth due to the chemical interaction with the substrate. The partially oxidized layer may change its structure (e.g., grain size, crystallinity) depending on the degree of the reaction and also the affect on the morphology of the Au film covering it. In the chemical etching process of the Ti and Cr films directly on the oxides, such chemical and physical fluctuations of the film structure as the result of the intrinsic chemical interaction with oxides should be considered. For instance, the etching time is expected to strongly depend on the degree of oxidization and the grain size of the metal film.
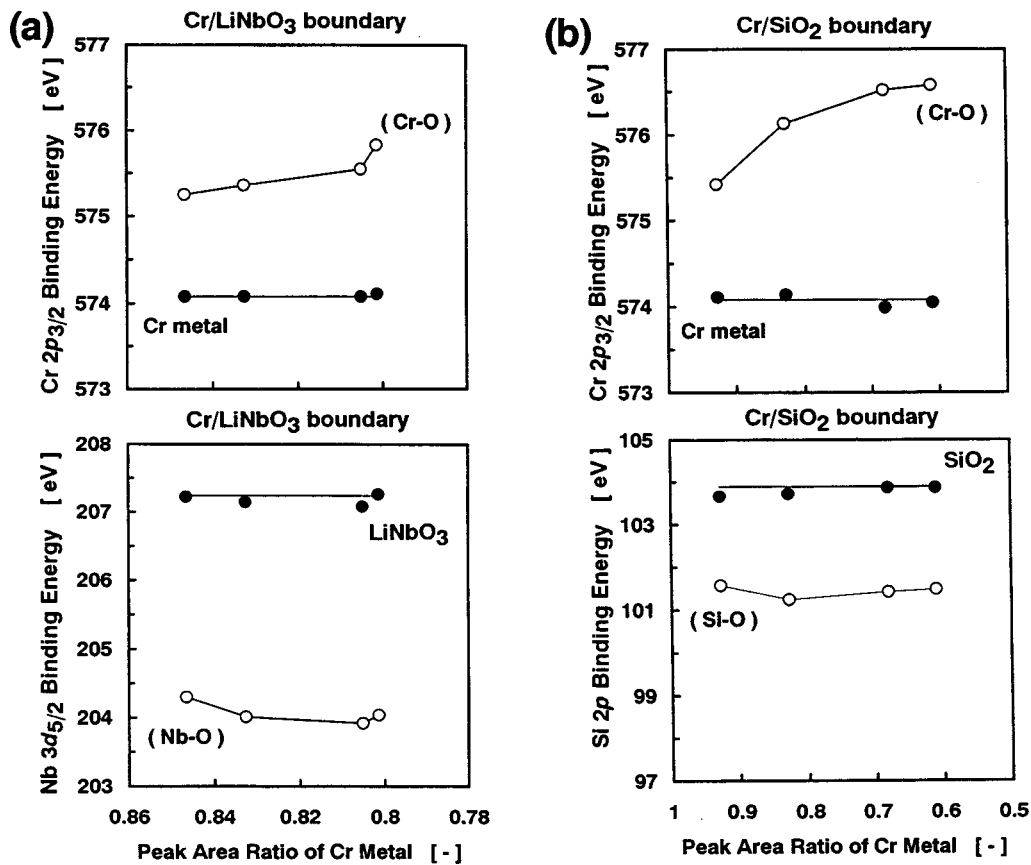
FIG. 15. XPS chemical shift measured on Cr $2p_{3/2}$ and Nb $3d_{5/2}$ peaks of the Cr/LiNbO$_3$ sample (a) and on Cr $2p_{3/2}$ and Si $2p$ of the Cr/SiO$_2$ /LiNbO$_3$ sample (b). The data were obtained at the points after 20, 22, 24, and 26 min of Ar-ion etching of Figs. 2(a) and 2(b) for the corresponding sample. The horizontal axes are plotted by an XPS peak area ratio of the metallic component not by the sputtering time calculated by (Cr $2p$)$_{metal}$ /[(Cr $2p$)$_{metal}$+(Cr $2p$)$_{oxides}$].

. ELECROCHEMICAL FAILURE IN ELECTRODES

As is generally known, if dissimilar materials are used for the electrodes, an electrochemical reaction such as the Galvanic cell reaction occurs, especially in moist atmosphere, and leads to a short circuit, etc. For instance, the Au/Cr binary film which is inserted sometimes between SiO$_2$ and the thick Au electrodes as the glue layer, is a combination of dissimilar materials. Nemirovsky, Blech, and Yahalom reported that the undercutting was caused by enhanced Au etching near the junction of the Au/Cr Galvanic cell.[6] Such a phenomenon is disadvantageous to maintaining the bonding strength of the electrodes during long-term device operation. The combination of Au/Si generates a short circuit when the biased device is operated in moist atmosphere: the Si layer is used in z-cut LiNbO$_3$ modulators to improve their temperature stability.

Figure 16 is the SEM images of the failed electrodes due to the short circuit occurring after several hours of operation under 95 %RH atmosphere at 80°C with a dc = 10 V biased state. The sample was an unsealed x-cut LiNbO$_3$ modulator device, in which the Au electrodes were formed on the SiO$_2$ buffer layer covering the LiNbO$_3$ using a Ti thin film as the glue layer. In this sample, an electrochemical reaction was thought to intensify the growth of precipitates (marked as " 1 " in Fig. 16) between the pair of electrodes and lead to a short circuit. Another similar device, the package of which

TABLE II. XPS, AES, and AFM measurement results on Au/Ti and Au/Cr binary films deposited on LiNbO$_3$ and SiO$_2$ /LiNbO$_3$ substrates.

	Oxidization of glue layer		Surface morphology of Au	
Sample	Oxygen content through film (at. %)	Oxygen content near interface with substrate	Grain size (nm)	Roughness: R_a (5×5 μm area) (nm)
Au/Ti/LiNbO$_3$	2–3	Similar	80–100	0.8
Au/Ti/SiO$_2$	4–5	Large increase	20–50	2.2
Au/Cr/LiNbO$_3$	3	Similar	10–50	1.8
Au/Cr/SiO$_2$	8–9	Increase	20–50	1.5
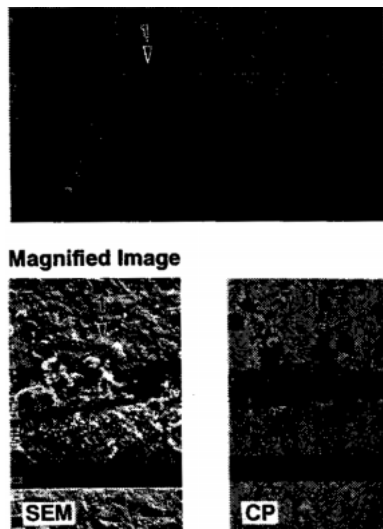
FIG. 16. SEM images of the failed Au electrodes. The gap distance between a pair of electrodes is 25 μm.

FIG. 17. AES analysis results on the precipitates appeared between the failed electrodes of Fig. 16, and the ordinary Au electrode surface.

had been hennetically sealed by metal welding and soldering, could be operated under the same condition without any failures.

Figure 1 7 reveals AES analysis results of the precipitates of Fig. 16, in which the AES result on an ordinary Au electrode is shown for comparison. The specific feature in the AES results of the precipitates between the electrodes, appeared in the shape of Au *NVV* peaks and in the peak intensity ratio of O to Au. The Ti peaks could not be detected by AES analyses from the precipitates. We consider that the above observation results were evidence of an electrochemical reaction at the Au electrodes and the generation of an oxidized or hydrated Au phase. Thus, there is the possibility that an electrolytic solution soaked the SiO_2 suface between the electrodes due to the moist atmosphere. In this regard, we checked whether inorganic anion contaminants existed in the electroplated Au electrodes by ion chromatography, but we could not find specific contaminants. At this moment, the best way to prevent such failures is to cut the immersion of moisture into the $LiNbO_3$ device surface by hermetic sealing of the device package.

. SUMMARY

In the production process of $LiNbO_3$ electro-optic devices, there is the possibility of many kinds of contaminants being left in the device constituent materials, resulting in poor device performance. Although the type of contamination depends on the process, a high level in the process qualification is needed to improve the device quality and reliability. Special consideration of device design and device packaging structure is also important not only to eliminate undesirable contaminants but also to reduce the effect of the existing contaminants on the device performance. Adopting a dry process, covering the SiO_2 Iayer with a passive film, packing the device chip in a hermetically sealed case, etc., is the way to improve the $LiNbO_3$ device quality.

ACKNOWLEDGMENT

[1] GR-468-CORE, *Generic Reliability Assurance Requirements for Opto-electronic Devices Used in Telecommunications Equipment* (Bellcore, Red Bank, NJ, 1998), Issue 1.
[2] T. Nozawa and S. Miyazawa, Jpn. J. Appl. Phys., Part 1 **35**, 107 (1996),
[3] A. M. Prokhorov and Yu. S. Kuz'minov, *Physics and Chemistry of Crystalline Lithium Niobate* (Hilger, Bristol, U.K.. 1990), Chap. 1 .
[4] *Handbook of Photoelectron Spectroscopy*, edited by J. Chastain (Perkin-Elmer, Eden Prairie, MN, 1992).
[5] K. Fueki, *Denkihagakn-Binran (Handbook of Electrochemistry)* (Maruzen, Tokyo, 1985), Chap. 2.
[6] Y. Nemirovsky, I. A. Blech, and J. Yahalom, J. Electrochem. Soc. **125**, 1177 (1978).